RSC Advances

ROYAL SOCIETY OF CHEMISTRY

www.rsc.org/advances

Capillary filling dynamics of polymer melts in nanopores: Experiments and rheological modelling

Bing-Yang Cao*, Min Yang, Guo-Jie Hu

Key Laboratory for Thermal Science and Power Engineering of Ministry of Education, Department of Engineering Mechanics, Tsinghua University, Beijing 100084, P.R. China

* Corresponding author: Tel/Fax: 86-10-6279-4531; E-mail: caoby@tsinghua.edu.cn

ABSTRACT: Understanding capillary filling dynamics in nanoconfined geometries is crucial in the nanotechnology fields, such as nanofluidic devices, lab-on-a-chip, 3D printers, porous nanomaterials. The spontaneous capillarity-driven flow behaviors of polyethylene (PE) melts through anodized aluminum oxide (AAO) nanopores are investigated experimentally by using the nanoporous template wetting technique first in our study. The diameter of the pores is 100 nm and 200 nm. The displacement of the polymer melts is measured by the thickness of the fabricated nanowire array as a function of time. Besides, considering the effect of the shear rate on the polymer viscosity in the capillary nanoflow, a theoretical model, i.e. a modified Lucas-Washburn law that combines the Lucas-Washburn law with the polymer rheological model, is established. Based on the experimental results it is speculated that the rise of the meniscus agrees with the modified Lucas-Washburn law. It also suggests that the zero-shear-rate viscosity of the PE melts decreases in their flows through the nanopores and the induced unconventional rheological behavior may be caused by nanoconfinement of the nanopores.

KEYWORDS: polymer melts, capillary flow, nanoporous template wetting, Lucas-Washburn law, rheological behavior

I. INTRODUCTION

The capillary flow of liquids through nanochannels plays a decisive role in a broad range of natural and industrial applications, such as nanofluidic devices, lab-on-a-chip systems and porous nanomaterials. In recent years, with the progress in micro/nanofluidics and nanotechnology, nanofluidic devices and nanostructures manufactured based on it have drawn more and more attention. Among them, polymer nanostructures, with several advantages over other materials, such as low cost, simple processing techniques and accurate repeatability in mass-production, have offered potential applications in many areas, such as photonics [1,2], mechatronics [3,4], medicine and fluidic nanodevices [5,6]. For the fabrication of these nanoproducts, a set of processing approaches, such as photolithography, scanning beam lithography [7], moulding [8], embossing [9], printing [10] and electrospinning [11] have been reported. Among these techniques, moulding offers a wide application and has the potential to be the ultimate low-cost method for manufacturing [12]. Besides, the thermal conductivity of the fabricated polymer nanowire arrays were found to be about 2 orders of magnitude higher than their bulk counterparts, and with the morphology of the micro- and nanostructures on the surface superhydrophobicity of polymers has been obtained [13,14]. As to fabricate high-quality polymer nanoproducts by nanomoulding, accurately controlling the flow behaviors of polymer melts through nanochannels is a key point [15].

For the capillary flow behaviors of liquids through pores, lots of theoretical, numerical and experimental studies [16-21] have been done in search of a thorough physical understanding of the basic mechanisms involved. Almost a century ago, Lucas and Washburn established the basic capillarity law for Newtonian liquids, i.e. the Lucas-Washburn equation (LWE) [16]

$$H(t)=\left(\frac{\gamma_{LV}R\cos\theta}{2\eta}\right)^{1/2}\sqrt{t}\,. \quad (1)$$

Here $H(t)$ is the rise of the fluid meniscus, t is the wetting time, γ_{LV} is the surface tension of the liquid, η is the viscosity, R is the pore radius and θ is the contact angle between the meniscus and the wall. The LWE predicts that the capillary rise should be proportional to the square root of time based on the assumption that the Poiseuille region covers practically the whole flow. Joos et al. [17] combined the LWE with an empirical relationship between the dynamic contact angle (DCA) and the capillary number and obtained a modified formula that showed better agreement with the experimental data, especially at short time. For the DCA, another commonly used model is the molecular-kinetic model proposed by Blake and Haynes [18] which gave the relationship between the DCA and the velocity. Recently, Zhmud et al. [19] pointed out some internal inconsistencies of the classical equation including the singularity in the zero-time limit, nonlinear dissipation and flow pattern effects in the front zone of the liquid column and near the capillary entrance. With the corrections that removed the initial infinite acceleration and considered the second-order dissipation effects they obtained a more general equation including higher order terms in the capillary rise. Besides, Levine et al. [20] developed a comprehensive mathematical theory of the hydrodynamics of the fluid motion in the reservoir near the capillary entrance and the departure from Poiseuille flow in the vicinity of the advancing meniscus. In the case of non-Newtonian liquids, Digilov [21] studied the impact of non-Newtonian behavior on the capillary rise dynamics of a power law liquid and got an analytical solution for the time evolution of the meniscus height which was checked against the results of experiments at millimeter scale.

Actually whether the Lucas-Washburn equation or the modified formulas are applicable at micro- or nanoscale is still under discussions. Some experiments and numerical simulations have been carried

out in recent years. Geromichalos et al. [22] investigated the spontaneous imbibition of water and 1-undecanol fronts between two roughened glass plates with the separation between 10 and 50 μm, while Gruener and Huber [23] studied the capillary filling behavior of water, liquid *n*-tetracosane and liquid crystal octyloxycyanobiphenyl in Vycor. Both of their work confirmed the LWE. Meanwhile, Oh et al. [24] found that the dynamics of the filling of nanochannels using mixtures of ethanol and water followed the $(\text{time})^{1/2}$ dependence but the prefactor of the algebraic relation greatly deviated from the predictions based on the LWE with the bulk properties. The $(\text{time})^{1/2}$ dependence of the filling height but quantitative deviation of the prefactor from the LWE were also reported by Engel and Stuhn [25] in their experimental measurements of the filling process in nanopores of polymer melts which appeared as Newtonian liquids in the shear experiment since their molar masses were well below the critical molecular mass of entanglement.

More numerical studies have been done but no consistent description of the filling behavior at nanoscale has been got. Quirke et al. [26,27] found out the penetration length was a linear function of time for short time and tended to a $(\text{time})^{1/2}$ dependence at long time based on their molecular dynamics (MD) simulations of carbon nanotubes imbibing decane. They believed that the linear time dependence at short time was due to the formation of a precursor film which spreaded at a much greater speed in advance of the main wetting line. However, Chibbaro et al. [28] found that the dynamics of the precursor films obeyed a square-root law although with a larger prefactor by both hydrokinetic and MD approaches. Martic et al. [29] demonstrated a reduction in the rate of penetration for a simple Lennard-Jones (LJ) fluid by using MD simulations and believed the reduction was caused by the contact angle that depended on the rate of wetting, especially during the early stages of capillary filling. There were lots of studies [30-36] on the filling of various liquids (e.g. LJ fluid, polymer, liquid

propane and water) into nanochannels (e.g. nanopores, patterned channels and carbon nanotubes) by using MD or lattice Boltzmann simulations. They observed the deviation of the kinetics of imbibition from the LWE and demonstrated the neglection of the DCA in the LWE is responsible for the deviation. Besides the DCA correction, some researchers investigated the effects of slip on the capillary dynamics and proposed the modifications to the LWE. Dimitrov et al. [37], using MD simulations, found for both the simple LJ fluid and polymer melts the meniscus rose according to the LWE after a transient period of a few nanoseconds. For the polymer melt, however, a slip length exhibited. Joly [38] even believed the standard description of capillary filling dynamics had to be modified to account for the liquid/solid slip in nanometric pores based on their MD simulations of dynamics of water uptake by carbon nanotubes. Recently, Bakli and Chakraborty [39] derived a universal analytical depiction of capillary imbibition characteristics of water in nanoscale pores through the realization of a molecularly sensitive closure model for dynamic slip length and they believed the DCA did not play any significant role in their work based on the simulation data of the contact angles which relaxed to the static value within a very short time span.

No reports on non-Newtonian liquids in nanoscale pores can be found in literature, especially experimental work, although it is a significant topic. There exists no description of the capillary flow behaviors of non-Newtonian liquids like polymer melts through nanopores that is experimentally and theoretically consistent. In our previous paper [40], the preliminary study showed that the capillary filling of PE melts into nanopores followed the LW model, in which we did not take into account the non-Newtonian characteristics of PE melts. Here we get more fruitful experimental data, and the aim of the present paper is to further clarify the problem of capillary filling of polymer melts in nanopores. We investigate the flow behaviors of the PE melt in AAO nanoporous templates experimentally, and

develop a modified LW model of the capillary flow of polymer melts through nanopores based on the experimental results considering the non-Newtonian characteristics. Here, our experiments are on much longer time scale compared with the existing MD studies, which is more instructive to practical applications.

II. EXPERIMENTAL DETAILS

Here we use the nanoporous template wetting technique to investigate the capillary flows of PE melts through nanopores. The AAO nanoporous templates used here are purchased from Whatman, Inc.. The templates are freestanding disks with a diameter of 13 mm. Their pores are all through-holes with a length of 60 μm and two batches of diameters of 200 nm and 100 nm. The top view and cross-section images, characterized by scanning electron microscopy (SEM, Hitachi S-5500), of the AAO nanoporous template with the pore diameters of 200 nm are given in Fig. 1(a) and 1(b), respectively. The PE films with thickness of about 300 μm, density of 0.945 g/cm^3 are obtained from Qilu Petroleum and Chemical Co. of China.

In the experiments, a PE film is placed on the top of the template with a good contact and then put into a chamber in vacuum with the temperature of 130 °C at which the PE film will melt and infiltrate into the nanopores of the template. After a period of time the PE nanowire array with certain thickness can be produced. Choosing different wetting time we get the nanowire arrays with different thicknesses, i.e. the different wetting displacements of the PE melt. Then, the sample is taken out of the chamber and cooled down to ambient temperature. After that, the PE nanowire array is released by removing the template in NaOH aqueous solution and being rinsed with deionized water and ethanol in sequence. At last, the sample is dried at 30 °C in vacuum. Here, the thicknesses of the nanowire arrays are surely

reflect the nanoflow velocity of the PE melt.

The top view and cross-section SEM images of the as-fabricated PE nanowire array generated within the AAO nanoporous template with a pore diameter of 200 nm after being heated at the wetting temperature of 130 °C for 30 min are shown in Fig. 1(c) and 1(d), respectively. By measuring the cross-section SEM image, we can get the thickness of the nanowire array. As to ensure the accuraty of our results, three repeatability experiments for each wetting time are carried out and the final data are obtained by averaging over the three samples as well as more than five positions on each sample. Using this method, we also get the thicknesses of the nanowire arrays generated at other different wetting time.

Besides, the dependence of the viscosity of the PE sample used in our experiment on the shear rate at 130 °C is measured by a standard rotor rheometer (Physica MCR300) and the detailed results can be found in Ref [40]. The range of the stress strain rate that the rotor rheometer applies on the sample is consistent with that exists in the nanoflow in our experiment. A comparison is made between the measured values and the Carreau model (CM) [41,42],

$$\eta(\dot{\gamma}) = \frac{\eta_0}{\left[1+(\lambda\dot{\gamma})^2\right]^q}, \tag{2}$$

which was developed empirically from the behaviors of complex fluids. In Eq. (2), η_0 is the zero-shear-rate viscosity and the parameter λ is a characteristic time constant, approximately equal to the inverse of the strain rate when shear thinning behavior begins. The fitting parameters are estimated to be η_0=2.95×10^5 Pa·s, λ=63 s and q=0.26, consistent with the reference [43].

III. RESULTS AND DISCUSSION

In order to discuss the experimental data of the displacements of the PE melt, we develop a theoretical

model first since the classical LWE is applicable only for Newtonian fluids. As shown in Fig. 2, the effect of the shear rate on the viscosity should be considered for the PE sample which exhibits shear thinning behavior. Thus, the LWE that is a Newton dynamics equation [19] is not applicable here and we should derive the dynamics equation for Carreau fluids. Based on the assumption of a quasi-steady process and unidirectional flow, the equation of motion [44] reads

$$-\frac{\partial p}{\partial z}+\frac{1}{r}\frac{\partial}{\partial r}\left(r\tau_{rz}\right)=0, \tag{3}$$

where z is the axial position, r is the radial position, $\partial p/\partial z$ is the pressure gradient along the cylinder and τ_{rz} is the shear stress. For Carreau fluids, the shear stress can be described as

$$\tau_{rz}=\eta\left(\dot{\gamma}\right)\dot{\gamma}=\frac{\eta_0}{\left[1+\left(\lambda\frac{\partial v}{\partial r}\right)^2\right]^q}\frac{\partial v}{\partial r}, \tag{4}$$

where $\dot{\gamma}$ is the shear rate, v is the velocity in the axial direction. By substituting Eq. (4) into Eq. (3), the equation of motion can be rewritten as

$$-\frac{\partial p}{\partial z}+\frac{1}{r}\frac{\partial}{\partial r}\left(r\frac{\eta_0}{\left[1+\left(\lambda\frac{\partial v}{\partial r}\right)^2\right]^q}\frac{\partial v}{\partial r}\right)=0. \tag{5}$$

In capillary, the pressure gradient is obtained by taking into account that $p|_{z=0}=0$ and $p|_{z=H(t)}=2\gamma_{\mathrm{LV}}\cos\theta/R$:

$$\frac{\partial p}{\partial z}=\frac{2\gamma_{\mathrm{LV}}\cos\theta}{RH\left(t\right)}. \tag{6}$$

In a quasi-steady process, at certain time t the meniscus height $H(t)$ is a given value. Therefore the pressure gradient will be a constant. Then, by integrating Eq. (5), we get

$$\eta_0\frac{\mathrm{d}v}{\mathrm{d}r}=\frac{\gamma_{\mathrm{LV}}r\cos\theta}{RH\left(t\right)}\left[1+\left(\lambda\frac{\mathrm{d}v}{\mathrm{d}r}\right)^2\right]^q, \tag{7}$$

where $H(t) = v_m t = \frac{2t}{R^2}\int_0^R vrdr$ with the mean velocity v_{m}. The solution of Eq. (7) can be carried out numerically through finite differences. Comparing the above derivation with that of the LWE, it can be seen that if the effect of the shear rate is neglected the solution of Eq. (7) will reduce to the LWE. The solution is a modified LWE (MLWE) combining the LWE with the rheological model.

To obtain the theoretical results, it is crucial to determine the parameters firstly. Here, R is the pore radius (100 nm or 50 nm). The surface tension of polymer melts can be measured by the pendant drop method which was firstly reported by Wu [45]. He measured the surface tensions of polymer melts in the temperature range of 100 °C to 200 °C and the results could be expressed as a function of temperature. For PE, the function is

$$\gamma_{\mathrm{LV}} = 35.562 - 0.057(T - 20), \tag{8}$$

where the surface tension value γ_{LV} is in dyn/cm and the temperature T is in °C. Thus, we can get the surface tension of the PE melt at 130 °C is 29.3 dyn/cm (0.0293 $\mathrm{N \cdot m^{-1}}$). In our study, the capillary refers to the nanopore of the AAO templates with a high-energy surface, and the polymer melts with low surface energy can completely wet it. According to the Young's law [46] which can be expressed as

$$\cos\theta = \frac{\gamma_{\mathrm{SV}} - \gamma_{\mathrm{SL}}}{\gamma_{\mathrm{LV}}}, \tag{9}$$

where γ_{SV}, γ_{SL} and γ_{LV} represent the solid-vapor, solid-liquid and liquid-vapor interfacial tensions, respectively, θ will be a very small value for the complete wetting. Here, we take θ=10 ° based on the property of aluminum oxide. Besides, in order to compare the theoretical results with the experimental data conveniently, we set the initial condition of the finite-difference procedure same as the experiments. The theoretical solutions and our experimental data of the displacements of the PE melt $H(t)$ at different wetting time are shown in Fig. 2. The experimental data in Fig. 2 have been modified

to ascertain the starting time is from t=0 by both CFD simulations and theoretical analyses of the thermal inertia of the sample.

As can be seen in figure 2, the $H(t) - t^{0.5}$ dependence is not linear for both our experimental data and the theoretical solutions of the MLWE. For the LWE, the viscous drag is a linear function of velocity, which results in a linear relationship between $H(t)$ and $t^{0.5}$ [19], while for Carreau fluids the viscous drag is a nonlinear function of velocity, and the dependence of $H(t)$ on $t^{0.5}$ will be nonlinear. Thus, our MLWE instead of the LWE can model the capillary filling dynamics of polymer metls in nanopores. However, it also can be seen in figure 2 that the nanoflow velocity of polymer melts measured in our experiments is much larger than that predicted by the MLWE using the measured parameters. As mentioned before, some corrections, such as the slip [37-39] and DCA [29,30,33], have already been proposed and we will analyze their effects on the nanoflows of polymer melts here.

Assuming the wall slip l_s exists in the flow, the velocity at the position apart l_s from the capillary wall equals zero. It is believed that the slip length vanishes for a completely wetting surface, but increases with the contact angle. When the contact angle goes to 180°, the slip length diverges as [47,48]

$$l_s/\sigma \sim 1/(\pi - \theta)^4 , \quad (10)$$

where l_s is the slip length and σ is the molecular diameter. In our case, the contact angle θ is about 10°. The molecular diameter is taken as the radius of rotation of the polymer chain and for the PE the value is about 5.62 nm [49]. Then, the slip length can be estimated to be about 0.0725 nm. The theoretical solutions considering the effect of the certain wall slip are presented in Fig. 3. It can be seen that the theoretical solutions still deviate far from the experimental data and the wall slip correction of the MLWE is very small, specifically less than 0.5%. Thus, we believe the wall slip cannot explain our

experimental results.

To discuss the effect of the DCA, two commonly used models (i.e. hydrodynamic and molecular-kinetic models) are employed to calculate the DCA. In the context of the hydrodynamic model, the most complete analysis is the Cox equation [50] as follows:

$$\theta_{\mathrm{d}} = \left(\theta_{\mathrm{e}}^{3} + 9A \frac{\eta}{\gamma_{\mathrm{LV}}} \frac{\mathrm{d}H}{\mathrm{d}t} \right)^{1/3} \tag{11}$$

and $A = \ln\left(R/\delta\right)$, where δ is the slip length of the meniscus, θ_{d} and θ_{e} denote the DCA and equilibrium contact angle (ECA), respectively. In our calculations, θ_{d} and θ_{e} are often expressed in radian, R and δ are in nm, γ_{LV} is in dyn/cm, η is in mPa·s and dH/dt is in m/s. The contact angle θ mentioned before denotes the ECA. According to the molecular-kinetic (MK) model [18], which excludes the viscous dissipation and takes the solid surface characteristics into account so that the energy dissipation occurs only at the moving contact line, the relationship between θ_{d} and the velocity of the wetting line dH/dt reads

$$\cos\theta_{d} = \cos\theta_{e} - \zeta \frac{\eta}{\gamma_{\mathrm{LV}}} \frac{\mathrm{d}H}{\mathrm{d}t} \tag{12}$$

and $\zeta = \dfrac{nk_{\mathrm{B}}T\Omega_{\mathrm{L}}}{h\kappa_{\mathrm{S}}^{0}\lambda}$ **is a coefficient of friction per length of the contact line depending on both fluid viscosity and liquid solid interaction**, where n is the number of adsorption sites per unit area, k_{B} is the Boltzmann constant, T is the absolute temperature, Ω_{L} is the volume of the 'unit of flow', h is Planck's constant, λ is the length of the individual molecular displacements near the contact line, κ_{S} is the frequency of the individual molecular displacements that occur along its length. Then, by replacing θ in Eq. (7) with θ_{d} obtained in Eq. (11) or (12), we can obtain the theoretical solution of the MLWE considering the DCA. The slip length of the meniscus δ in the Cox equation and dimensionless parameter ζ in the MK model are the adjustable parameters. Here, we just present one case for each DCA model, which is δ of d/4 and ζ of 10. The results are presented in Fig. 3. As shown in figure 3, the

theoretical solutions for the two DCA models both deviate far from the experimental data. In our calculations, we also obtain the solutions with the parameters δ and ζ taking other values. The extreme cases are that $\delta=d/2$ and $\zeta=0$ where the DCA is reduced to the ECA. The solutions show that $H(t)$ rises slower in all other cases than in those extreme cases, which is consistent with the reports [29,30,33] and reasonable since the DCA is larger than the ECA. However, even the rise obtained in those extreme cases is found to be much slower than that observed in our experiments. Thus, it is believed the rise predicted by the theoretical solutions considering the DCA cannot be consistent with our experiment results no matter what the values of the parameters δ and ζ take.

It is reported that the nanoflow that is constrained by the nanoconfinement of the pore will strongly influence transport coefficients. Cao et al. [13] presented that the thermal conductivities of the PE nanowire arrays prepared in the same way were about 2 orders of magnitude higher than their bulk counterparts. Considering the relevance of the thermal conductivity and viscosity, we believe the zero-shear-rate viscosity of the PE melt will decrease in nanoflows. By fitting the MLWE with the experimental data, we get the zero-shear-rate viscosity η_0 are about 6.35×10^4 Pa·s and 5.25×10^4 Pa·s for the pores with diameters of 200 nm and 100 nm, respectively, which are both smaller than that of the bulk sample measured by rotor rheometer. As can be seen in figure 2, good agreement is observed between the fitted MLWE and the experimental data and the zero-shear-rate viscosity for the pore with a diameter of 100 nm is smaller than that for the 200 nm pore. We believe that the unconventional rheological behavior is induced by the nanoconfinement, i.e. the interaction between polymer chains and the alumina pore's wall with high surface energy, and the confinement is stronger for smaller pores. Based on the investigation of the morphologies of polymers in nanotubes and nanorods, the effect of the spatial confinement on the orientation of the polymer crystals has been reported. It was found that

the PE crystals developed in the AAO nanoporous template grew along the long axis of cylindrical nanopores restricted [51]. In addition, it was observed that the crystallites of poly(vinylidene difluoride) (PVDF) grew preferentially in the tube direction when the nanotubes were prepared by wetting the template with PVDF melts and the orientation of the PVDF chains prior to crystallization was speculated to be responsible for the difference in the crystallinity observed [52]. It has also been reported that the PVDF crystallized in the nanotrenches orients with the chain axis parallel to the walls [53]. Besides, the molecular simulations of polymer crystallization confined in rigid nanotubes also showed that the crystal orientation was uniform and parallel to the tube axis [54]. Given the anisotropic structure of polymer crystals described above, the orientation contributed to the nanoconfinement will decrease the viscosity, just like shear thinning.

IV. CONCLUDING REMARKS

In this paper, we have studied the flow behaviors of PE melts through nanopores experimentally by using the nanoporous template wetting technique. Based on the experimental results we find the displacement of polymer melts changes nonlinearly with $(\text{time})^{1/2}$, indicating the breakdown of the LWE that predict a linear relationship between the displacement and $(\text{time})^{1/2}$. A modified LWE is proposed by combining the rheological model of shear rate dependent viscosity. Comparing the experimental results and the theoretical solution of the MLWE quantitatively, we observe the decrease of the zero-shear-rate viscosity of polymer melts during their flows through nanopores, which means the polymer melts exhibit unconventional rheological behavior except the shear thinning in the nano-wetting process. As for the underlying mechanism of the unconventional rheological behavior we believe the intrinsic confinement of nanopores plays a dominant role.

ACKNOWLEDGMENTS

This work is financially supported by National Natural Science Foundation of China (No. 51322603, 51136001, 51356001), Science Fund for Creative Research Groups (No. 51321002).

REFERENCES

[1] Li G, Shrotriya V, Huang J, Yao Y, Moriarty T et al (2005) High-efficiency solution processable polymer photovoltaic cells by self-organization of polymer blends. Nat Mater 4: 864-868.

[2] Nie Z, Kumacheva E (2008) Patterning surfaces with functional polymers. Nat Mater 7: 277-290.

[3] Liu C (2007) Recent developments in polymer MEMS. Adv Mater 19: 3783-3790.

[4] Ryan AJ (2008) Nanotechnology: Squaring up with polymers. Nature 456: 334-336.

[5] Bruening M, Dotzauer D (2009) Polymer films: Just spray it. Nat Mater 8: 449-450.

[6] Zhou K, Zhu XG, Li Y, Liu J (2014) Fabrication of PDMS micro through-holes using micromolding in open capillaries. RSC Adv 4: 31988-31993.

[7] Gates DB, Xu Q, Stewart M, Ryan D, Willson CG et al (2005) New approaches to nanofabrication: molding, printing, and other techniques. Chem Rev 105: 1171-1196.

[8] Xia YN, Kim E, Zhao XM, Roger JA, Prentiss M et al (1996) Complex optical surfaces formed by replica molding against elastomeric masters. Science 273: 347-349.

[9] Chou SY, Krauss PR, Renstrom PJ (1996) 25-nanometer resolution. Science 272: 85-87.

[10] Xia Y, Rogers JA, Paul KE, Whitesides GM (1999) Unconventional methods for fabricating and patterning nanostructures. Chem Rev 99: 1823-1848.

[11] Li D, Xia Y (2004) Direct fabrication of composite and ceramic hollow nanofibers by

electrospinning. Nano Lett 4: 933-938.

[12] Attia UM, Marson S, Alcock JR (2009) Micro-injection moulding of polymer microfluidic devices. Microfluid Nanofluid 7: 1-28.

[13] Cao BY, Li YW, Kong J, Chen H, Xu Y et al (2011) High thermal conductivity of polyethylene nanowire arrays fabricated by an improved nanoporous template wetting technique. Polymer 52: 1711-1715.

[14] Cao BY, Kong J, Xu Y, Yung KL, Cai A (2013) Polymer nanowire arrays with high thermal conductivity and superhydrophobicity fabricated by a nano-molding technique. Heat Transfer Eng 34: 131-139.

[15] Beard JD, Rouholamin D, Farmer BL, Evans KE, Ghita OR (2015) Control and modelling of capillary flow of epoxy resin in aligned carbon nanotube forests. RSC Adv 5: 39433-39441.

[16] Washburn EW (1921) The dynamics of capillary flow. Phys Rev 17: 273-283.

[17] Joos P, Remoortere P, Bracke M (1990) The kinetics of wetting in a capillary. J Colloid Interface Sci 136: 189-197.

[18] T. D. Blake, J. M. Haynes, Kinetics of liquidliquid displacement, J. Colloid Interface Sci. 30 (1969) 421-423.

[19] Zhmud BV, Tiberg F, Hallstensson K (2000) Dynamics of capillary rise. J Colloid Interface Sci 228: 263-269.

[20] S. Levine, J. Lowndes, E. J. Watson, G. Neale, A theory of capillary rise of a liquid in a vertical cylindrical tube and in a parallel-plate channel: Washburn equation modified to account for the meniscus with slippage at the contact line, J. Colloid Interface Sci. 73 (1980) 136-151.

[21] Digilov RM (2008) Capillary rise of a non-Newtonian power law liquid: impact of the fluid rheology and dynamic contact angle. Langmuir 24: 13663-13667.

[22] Geromichalos D, Mugele F, Herminghaus S (2002) Nonlocal dynamics of spontaneous imbibition fronts. Phys Rev Lett 89: 104503.

[23] Gruener S, Huber P (2009) Spontaneous imbibition dynamics of an n-alkane in nanopores: Evidence of meniscus freezing and monolayer sticking. Phys Rev Lett 103: 174501.

[24] Oh JM, Faez T, de Beer S, Mugele F (2010) Capillarity-driven dynamics of water–alcohol mixtures in nanofluidic channels. Microfluid Nanofluid 9: 123-129.

[25] Engel M, Stuhn B (2010) In situ small angle x-ray scattering measurements of the filling process of polyisobutylene and poly-epsilon-caprolactone in ion track etched polycarbonate nanopores. J Chem Phys 132: 54-58.

[26] Supple S, Quirke N (2003) Rapid Imbibition of Fluids in Carbon Nanotubes. Phys Rev Lett 90: 214501.

[27] Whitby M, Quirke N (2007) Fluid flow in carbon nanotubes and nanopipes. Nat Nanotechnol 2: 87-94.

[28] Chibbaro S, Biferale L, Diotallevi F, Succi S, Binder K et al (2008) Evidence of thin-film precursors formation in hydrokinetic and atomistic simulations of nano-channel capillary filling. Europhys Lett 84: 605-609.

[29] Martic G, Gentner F, Seveno D, Coulon D, Coninck JD et al (2002) A molecular dynamics simulation of capillary imbibition. Langmuir 18: 7971-7976.

[30] Stukan MR, Ligneul P, Crawshaw JP, Boek ES (2010) Spontaneous imbibition in nanopores of different roughness and wettability. Langmuir 26: 13342-13352.

[31] Kusumaatmaja H, Pooley CM, Girardo S, Pisignano D, Yeomans JM (2008) Capillary filling in patterned channels. Phys Rev E 77: 601-611.

[32] Cupelli C, Henrich B, Glatzel T, Zengerle R, Moseler M et al (2008) Dynamic capillary wetting studied with dissipative particle dynamics. New J Phys 10: 1131-1137.

[33] Ahadian S, Kawazoe Y (2009) A molecular dynamics approach to examine the kinetics of the capillary imbibition of a polymer at nanoscale. Colloid Polym Sci 287: 961-967.

[34] Ahadian S, Mizuseki H, Kawazoe Y (2010) Prediction and analysis of flow behavior of a polymer melt through nanochannels using artificial neural network and statistical methods. J Colloid Interface Sci 352: 319-329.

[35] Wolf FG, dos Santos LOE, Philippi PC (2010) Capillary rise between parallel plates under dynamic conditions. J Colloid Interface Sci 344: 171-179.

[36] Stroberg W, Keten S, Liu WK (2012) Hydrodynamics of capillary imbibition under nanoconfinement. Langmuir 28: 14488-14495.

[37] Dimitrov DI, Milchev A, Binder K (2007) Capillary rise in nanopores: molecular dynamics evidence for the Lucas-Washburn equation. Phys Rev Lett 99: 054501.

[38] Joly L (2011) Capillary filling with giant liquid/solid slip: dynamics of water uptake by carbon nanotubes. J Chem Phys 135: 214705.

[39] Bakli C, Chakraborty S (2012) Capillary filling dynamics of water in nanopores. Appl Phys Lett 101: 153112.

[40] Hu GJ, Cao BY (2013) Flows of polymer melts through nanopores: Experiments and modelling. J Thermal Sci Tech, 8: 363.

[41] Carreau PJ (1972) Rheological equations from molecular network theories. Trans Soc Rheol 16: 99-127.

[42] Cao BY, Dong RY (2012) Nonequilibrium molecular dynamics simulation of shear viscosity by a

uniform momentum source-and-sink scheme. J Comput Phys 231: 5306-5316.

[43] Wu QY, Wu JA (2002) Polymer Rheology. Beijing: Higher Education Press.

[44] Landau LD, Lifshitz EM (1959) Fluid Mechanics. Oxford: Pergamon.

[45] Wu S (1970) Surface and interfacial tensions of polymer melts. II. Poly (methyl methacrylate), poly (n-butyl methacrylate), and polystyrene. J Phys Chem 74: 632-638.

[46] Young T (1805) Analysis of Interfacial Forces. Philos Trans Royal Soc London 95: 65-69.

[47] Priezjev NV, Troian SM (2004) Molecular origin and dynamic behavior of slip in sheared polymer films. Phys Rev Lett 92: 018302.

[48] Cao BY, Sun J, Chen M, Guo ZY (2009) Molecular momentum transport at fluid-solid interfaces in MEMS/NEMS: a review. Int J Mol Sci 10: 4638-4706.

[49] Benoit H (1976) Determination of polymer chain conformation in amorphous polymers. J Macromol Sci B 12: 27-40.

[50] Cox RG (1986) The dynamics of the spreading of liquids on a solid surface. Part 1. Viscous flow. J Fluid Mech 168: 169-194.

[51] Shin K, Woo E, Jeong YG, Kim C, Huh J et al (2007) Crystalline structures, melting, and crystallization of linear polyethylene in cylindrical nanopores. Macromolecules 40: 6617-6623.

[52] Steinhart M, Senz S, Wehrspohn RB, Gosele U, Wendorff JH (2003) Curvature-directed crystallization of poly (vinylidene difluoride) in nanotube walls. Macromolecules 36: 3646-3651.

[53] Hu ZJ, Baralia G, Bayot V, Gohy JF, Jonas AM (2005) Nanoscale control of polymer crystallization by nanoimprint lithography. Nano Lett 5: 1738-1743.

[54] Ma Y, Hu W, Hobbs J, Reiter G (2008) Understanding crystal orientation in quasi-one-dimensional polymer systems. Soft Matter 4: 540-543.

FIGURE CAPTIONS

FIG. 1 SEM images of the AAO nanoporous template with the pore diameter of 200 nm and the PE nanowire array generated after being heated at 130 °C for 30 min: (a) top view and (b) cross-section of the template; (c) top view and (d) cross-section of the array.

FIG. 2 Dependence of displacements of the PE melt on the square root of the wetting time obtained in our experiments and predicted by the MLWE.

FIG. 3 Dependence of displacements of the PE melt on the square root of the wetting time predicted by the MLWE considering the effect of the wall slip or DCA and our experiment data.

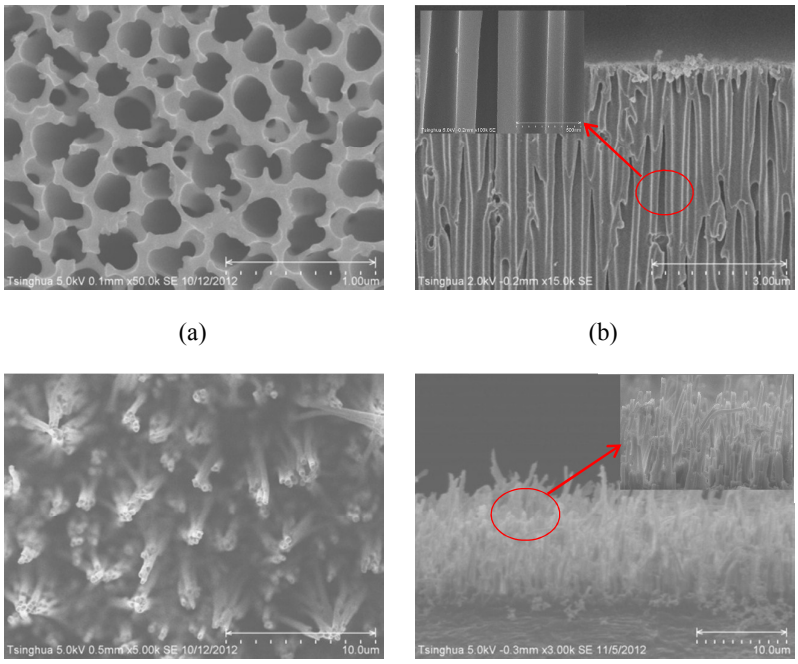

(a) (b)

(c) (d)

Figure 1

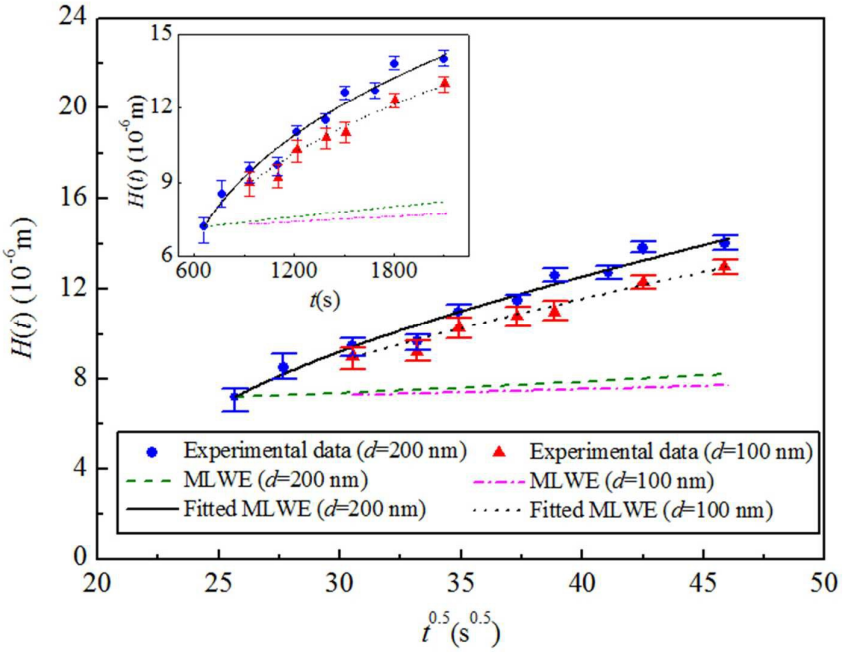

Figure 2

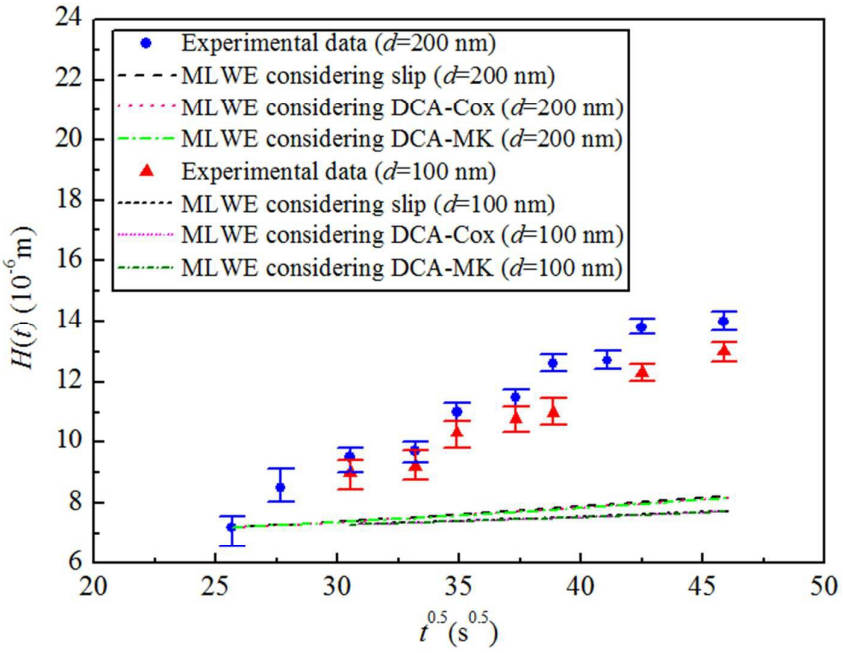

Figure 3

The spontaneous capillarity-driven flow behaviors of polyethylene (PE) melts through anodized aluminum oxide (AAO) nanopores suggest that the zero-shear-rate viscosity of the PE melts decreases in their flows, which can be predicted by a modified Lucas-Washburn law that combines the Lucas-Washburn law with the polymer rheological model.